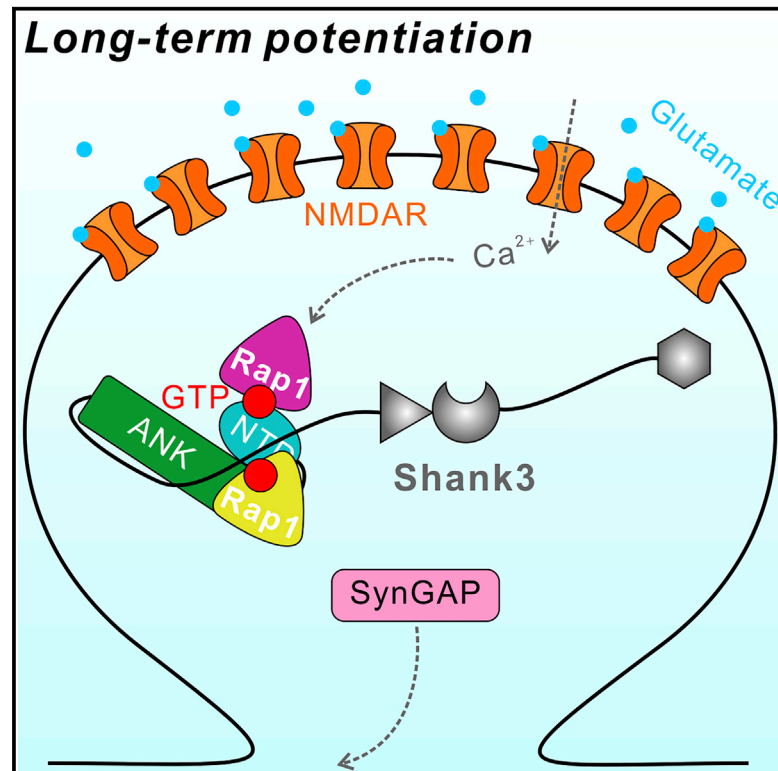


Structure

Shank3 Binds to and Stabilizes the Active Form of Rap1 and HRas GTPases via Its NTD-ANK Tandem with Distinct Mechanisms

Graphical Abstract



Authors

Qixu Cai, Tomohisa Hosokawa, Menglong Zeng, Yasunori Hayashi, Mingjie Zhang

Correspondence

mzhang@ust.hk

In Brief

Cai et al. report that Shank3 N-terminal NTD-ANK tandem forms an integral structural supramodule, binds to two copies of Rap1 with distinct modes, and prevents Rap1 GTP hydrolysis catalyzed by SynGAP.

Highlights

- Shank3 binds to Rap1 with an unexpected mode and a 1:2 stoichiometry
- Shank3 binds to HRas via a canonical binding mode and a 1:1 stoichiometry
- Binding of Shank3 prevents Rap1 GTP hydrolysis by SynGAP
- Binding of Shank3 to HRas or Rap1 is promoted upon synapse activation

Shank3 Binds to and Stabilizes the Active Form of Rap1 and HRas GTPases via Its NTD-ANK Tandem with Distinct Mechanisms

Qixu Cai,¹ Tomohisa Hosokawa,² Menglong Zeng,¹ Yasunori Hayashi,² and Mingjie Zhang^{1,3,4,*}

¹Division of Life Science, State Key Laboratory of Molecular Neuroscience, Hong Kong University of Science and Technology, Clear Water Bay, Kowloon, Hong Kong, China

²Department of Pharmacology, Kyoto University Graduate School of Medicine, Kyoto 606-8501, Japan

³Center of Systems Biology and Human Health, Hong Kong University of Science and Technology, Clear Water Bay, Kowloon, Hong Kong, China

⁴Lead Contact

*Correspondence: mzhang@ust.hk

<https://doi.org/10.1016/j.str.2019.11.018>

SUMMARY

Shank1/2/3, major scaffold proteins in excitatory synapses, are frequently mutated in patients with psychiatric disorders. Although the Shank N-terminal domain and ankyrin repeats domain tandem (NTD-ANK) is known to bind to Ras and Rap1, the molecular mechanism underlying and functional significance of the bindings in synapses are unknown. Here, we demonstrate that Shank3 NTD-ANK specifically binds to the guanosine triphosphate (GTP)-bound form of HRas and Rap1. In addition to the canonical site mediated by the Ras-association domain and common to both GTPases, Shank3 contains an unconventional Rap1 binding site formed by NTD and ANK together. Binding of Shank3 to the GTP-loaded Rap1 slows down its GTP hydrolysis by SynGAP. We further show that the interactions between Shank3 and HRas/Rap1 at excitatory synapses are promoted by synaptic activation. Thus, Shank3 may be able to modulate signaling of the Ras family proteins via directly binding to and stabilizing the GTP-bound form of the enzymes.

INTRODUCTION

SH3 and multiple ankyrin repeat domain (Shank) proteins (encoded by *SHANK1-3*) are major scaffolding proteins in excitatory postsynaptic densities (PSDs) (Naisbitt et al., 1999; Tu et al., 1999). All Shank proteins share similar domain organizations, each containing an N-terminal domain (NTD) with a “Ras-association domain” fold (Lilja et al., 2017; Mameza et al., 2013), an ankyrin repeats domain, an SH3 domain, a PDZ domain, a proline-rich sequence, and a C-terminal SAM domain (Figure 1A). Through direct and specific domain-domain interactions, such as binding to SAPAP (Zeng et al., 2016), Homer (Tu et al., 1999), and self-association by SAM (Baron et al., 2006) (Figure 1A), Shank proteins can form an extensive protein-protein interaction network in PSDs, which is critical for the formation,

maintenance and plasticity of PSDs (Hayashi et al., 2009; Kim and Sheng, 2004; Sheng and Hoogenraad, 2007; Ting et al., 2012; Tu et al., 1999; Zhu et al., 2016). Mutations of genes encoding Shank proteins are highly penetrant in causing psychiatric disorders, such as autisms and schizophrenia (Monteiro and Feng, 2017; Sala et al., 2015). For example, 22q13.3 deletions, leading to *SHANK3* haploinsufficiency, are known to cause Phelan-McDermid syndrome (Bonaglia et al., 2006). Overexpression of Shank3 has been implicated in hyperkinetic neuropsychiatric disorders (Han et al., 2013). Many point mutations of *SHANK3* have been identified in autism patients or individuals with intellectual disabilities (Durand et al., 2007; Gauthier et al., 2009; Moessner et al., 2007). Mutations of Shank genes in rodents often recapitulate many autism spectrum disorder (ASD) phenotypes, such as altered social behavior, anxiety-like phenotype, and obsessive-compulsive disorder-like repetitive behaviors (Peca et al., 2011; Schmeisser et al., 2012; Won et al., 2012; Zhou et al., 2019). Therefore, tremendous progress has been made in linking mutations in Shank genes and ASD via combined approaches of human genetics and animal model-based studies (Jiang and Ehlers, 2013; Leblond et al., 2014).

Structural studies showed that Shank NTD indeed couples with the ankyrin repeats to form an NTD-ANK supramodule (Lilja et al., 2017). Several proteins were identified to bind to the NTD-ANK tandem, and these proteins include Sharpin (Lim et al., 2001), α -fodrin (Bockers et al., 2001), HCN channel (Yi et al., 2016), and the guanosine triphosphate (GTP)-bound form of the Ras superfamily proteins of small GTPases (Lilja et al., 2017). However, the molecular basis governing the bindings of Shank NTD-ANK to any of these proteins are not known.

Small GTPases are critical regulators of synaptic plasticity. During long-term potentiation (LTP), small GTPases are activated by upstream Ca^{2+} signal and subsequently regulate diverse downstream signaling processes (Harvey et al., 2008; Hedrick et al., 2016; Murakoshi et al., 2011). There are several members of the Ras superfamily proteins, Ras and Rap, at excitatory synapses. These GTPases show a high amino acid sequence identity, adopt highly similar 3D structures, and share many common regulators/effectors or binding partners (Bos, 1998). Small GTPases are activated by guanine nucleotide exchange factors (GEFs) and inactivated by GTP-activating proteins (GAPs). Thus, GEFs and GAPs act as molecular switches

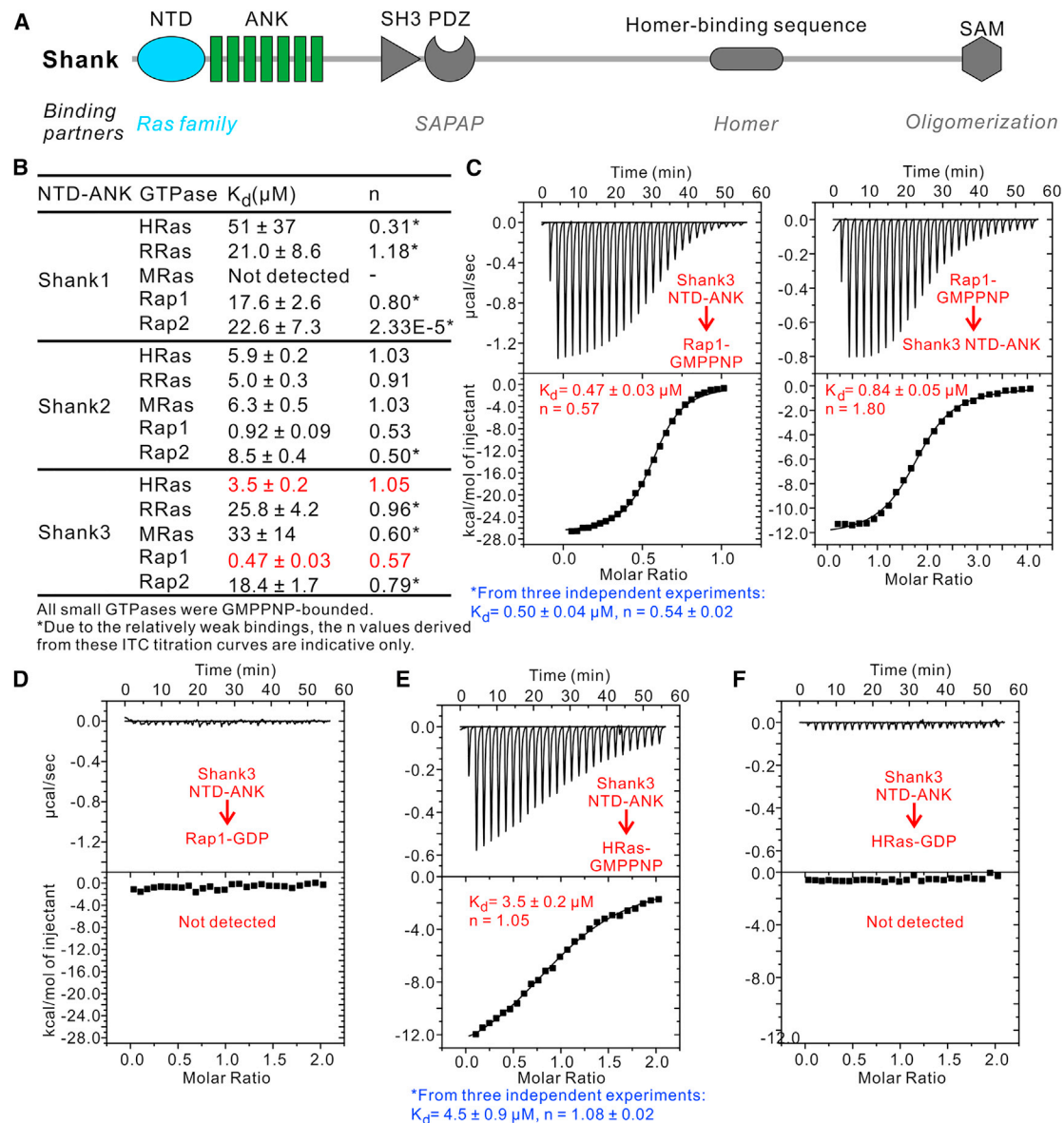


Figure 1. Specificity of the Interactions between Shank Proteins and Ras Superfamily Proteins

(A) Schematic diagram showing the domain organization of Shank proteins with selected binding partners for each domain indicated.

(B) Summary of ITC-based measurements of the binding affinities between the NTD-ANK tandems of Shank proteins and variant members of the Ras superfamily GTPases.

(C) Interaction between Shank3 and GMPPNP-bound Rap1 measured by ITC-based experiment. Left panel: 150 μ M Shank3 NTD-ANK in the syringe was titrated into 30 μ M GMPPNP-bound Rap1 in the cell. Right panel: 200 μ M GMPPNP-bound Rap1 in the syringe was titrated into 10 μ M Shank3 NTD-ANK in the cell. The fitted K_d and n value for the titration curve are indicated in red within the panel. We also report K_d and n values of the reaction in the format of mean \pm SD (in blue) by averaging three independent titration experiments using different batches of proteins; same as in (E).

(D) Interaction between Shank3 and GDP-bound Rap1 measured by ITC-based experiment. Shank3 NTD-ANK (150 μ M) in the syringe was titrated into 15 μ M GDP-bound Rap1 in the cell.

(E) Interaction between Shank3 and GMPPNP-bound HRas measured by ITC. Shank3 NTD-ANK (150 μ M) in the syringe was titrated into 15 μ M GMPPNP-bound HRas in the cell.

(F) Interaction between Shank3 and GDP-bound HRas measured by ITC-based experiment. Shank3 NTD-ANK (150 μ M) in the syringe was titrated into 15 μ M GDP-bound HRas in the cell.

See also Figure S1.

of GTPases. SynGAP, a highly abundant protein in PSDs, is a Ras/Rap GAP functioning to “turn off” Ras and Rap activities and therefore acts as an inhibitory factor to the functions of

the GTPases (Kim et al., 2003; Komiya et al., 2002). LTP induction rapidly disperses SynGAP from dendritic spines to shift the balance of Ras and Rap toward their active forms (Araki

et al., 2015). It is not known whether Shank binding to Ras/Rap functions merely as a scaffold to anchor the GTPases in PSDs or also directly modulate the activities of the enzymes. Indeed, Shank3 has been shown to sequester active Rap1 from activating integrin-mediated cell migrations in heterologous cells, suggestive of a regulatory role of the interaction (Lilja et al., 2017).

Here, we systematically studied the interactions between Shank proteins and the Ras family proteins using biochemical approaches. To understand the molecular mechanism governing their interactions, we solved the crystal structures of Shank3 NTD-ANK in complex with Rap1 or HRas. Unexpectedly, Shank3 interacts with Rap1 with a 1:2 stoichiometry through a canonical binding mode via the Ras-association domain and a previously unknown binding site where both NTD and ANK are involved in the binding. We also discovered that binding of Shank3 to Rap1 prevents SynGAP from activating GTP hydrolysis of Rap1. Finally, we demonstrated that the binding of Shank3 to HRas or Rap1 at excitatory synapses is promoted by glutamate-mediated synapse activation. Thus, the Shank and Ras superfamily interactions may play a role in sustaining the Ras/Rap activities in synapses.

RESULTS

Specificity of the Interactions between Shank Proteins and the Ras Superfamily Proteins

The Shank NTD was proposed to be a Ras-association domain that can directly interact with active (i.e., the GTP-bound form) Ras and Rap GTPases (Lilja et al., 2017). Using isothermal titration calorimetry (ITC)-based binding assays, we studied the specificity of the interactions between the Shank proteins and the Ras superfamily proteins. The NTD-ANK tandems of three members of Shank (Shank1, residues 73–440; Shank2, residues 49–423; and Shank3, residues 1–376) were purified and subjected to ITC experiments with several members of the Ras family GTPases (HRas, RRas, MRas, Rap1, and Rap2). Most pairs of interactions were relatively weak, except that the active form of Rap1 (i.e., the GMPPNP-bound form) binds to the NTD-ANK tandems from Shank2 and Shank3 with submicromolar dissociation constants (Figures 1B and 1C). Importantly, the GDP-bound Rap1 had no detectable binding to Shank NTD-ANK (Figure 1D). Unexpectedly, the binding ratio between Rap1 and the NTD-ANK tandem of Shank2 or Shank3 is 2:1 (Figures 1B, 1C, and S1A). In contrast, the binding between the GMPPNP-bound form of HRas and Shank3 NTD-ANK, the next strongest interaction, displayed a 1:1 stoichiometry under the same condition by ITC (Figure 1E), and the binding between HRas and Shank3 NTD-ANK is also strictly limited to the GTP-bound form of HRas (Figure 1F). Thus, Rap1 and HRas, two highly similar members of the Ras superfamily GTPases, behave differently when binding to the Shank proteins.

Analytical gel filtration chromatography coupled with multi-angle light scattering assay was also used to evaluate the bindings of Shank3 NTD-ANK to Rap1 and HRas. For the Shank3/HRas interaction, increase the molar ratio of HRas to Shank3 from 1:1 to 2:1 did not further alter the elution volume of the complex (Figures S1B and S1C). In contrast, for the Shank3/Rap1 interaction, increase of the molar ratio of Rap1 to Shank3

from 1:1 to 2:1 further shifted the complex elution peak to a smaller volume. Further increase of Rap1 did not alter the elution volume of the complex anymore (Figures S1B and S1C), indicating that each Shank3 NTD-ANK binds to more than one Rap1.

The Structure of Shank3 NTD-ANK in Complex with Rap1 Reveals a Canonical and a Non-canonical Rap1 Binding Sites in Shank3

To elucidate the molecular basis underlying the interaction between Rap1 and Shank3, we solved the crystal structure of Shank3 NTD-ANK in complex with GMPPNP-bound Rap1 to the resolution of 2.81 Å (Table 1). Consistent with our ITC-based assay (Figure 1), two GMPPNP-bound Rap1 molecules binds to one molecule of Shank3 NTD-ANK with two distinct binding surfaces (Figures 2A and 2B).

The structure of Shank3 NTD-ANK in complex with Rap1 is essentially the same as that of the apo-form NTD-ANK (Lilja et al., 2017) (PDB: 5G4X, an overall root-mean-square deviation of 0.566 Å between the C α atoms of two structures). Two Rap1 binding sites on Shank3 NTD-ANK are non-overlapping with each other. The first Rap1 binding site is via the canonical Ras-association domain of NTD as predicted (Lilja et al., 2017) (Figure 2C). Superposition of Rap1/Shank3-NTD complex with complex structures of Rap1 and Ras with other association proteins, such as cRaf1, KRIT1, and RIAM, revealed a nearly identical binding mode (Figure S3A). In this canonical binding, part of the “switch I” region of Rap1 form an antiparallel β sheet with the second β strand of Shank3 NTD, forming an extended inter-molecular β sheet (Figures 2A, right and S3A). In addition to the backbone hydrogen bonds formed by the inter-molecular β strand pairing, the binding between Rap1 and Shank3 NTD also involves a hydrogen bond formed between side chains of K22_{Shank3} and Y40_{Rap1} and a salt bridge between R12_{Shank3} and E37_{Rap1} (Figure 2C). Both K22 and R12 are highly conserved in all members of the Shank family (Figure S2), indicating that the canonical binding site is likely to be common for all Shank proteins. For the canonical interaction with Ras-association domains, Rap1 normally has two additional salt bridge interactions involving K31_{Rap1} and D33_{Rap1}, binding to a negatively charged and a positively charged residues in Ras-association domains, respectively (Huang et al., 1998; Nassar et al., 1995). However, the corresponding residues in Shank3 NTD are C41_{Shank3} and A42_{Shank3}, which cannot form electrostatic interactions with K31_{Rap1} and D33_{Rap1}. A negatively charged residue corresponding to C41_{Shank3} in Ras-association domain is considered as the major determinant for their specific binding to HRas or Rap1 (Nassar et al., 1996), but this is apparently not the case for the interaction between Shank3 NTD and Rap1.

We next purified isolated Shank3 NTD to study its binding to Rap1 as a way to dissect the role of the NTD-ANK supramodule in Rap1 binding. GMPPNP-bound Rap1 was found to bind to Shank3 NTD with a $K_d \sim 0.41 \mu\text{M}$ and a 1:1 stoichiometry (Figure S3B), indicating that the canonical form of the binding between Rap1 and Shank3 NTD is independent of ANK. Substitution of K22_{Shank3}, the residue critical for the interaction between Shank3 NTD and Rap1 (Figure 2C), with either Glu or Ala completely disrupted the NTD/Rap1 interaction. Substitution

Table 1. Crystallographic Data Collection and Refinement Statistics

	Shank3 NTD-ANK/Rap1	Shank3 NTD-ANK- A42K/HRas
Data Collection		
Space group	C2	P2 ₁
Wavelength (Å)	0.97918	0.91904
Unit cell parameters		
a, b, c (Å)	171.032, 54.107, 203.110	80.569, 154.464, 116.949
α, β, γ (°)	90, 109.513, 90	90, 108.347, 90
Resolution range (Å)	50–2.81 (2.86–2.81)	50–3.30 (3.36–3.30)
No. of unique reflections	40,063 (1,812)	40,509 (2,006)
Redundancy	6.1 (5.6)	3.4 (3.2)
I/σ	9.64 (1.04)	3.57 (1.00)
Completeness (%)	94.0 (85.4)	99.3 (98.9)
R _{merge} ^a (%)	15.0 (94.8)	23.2 (73.7)
CC _{1/2} ^b	0.984 (0.757)	0.939 (0.546)
Structure Refinement		
Resolution (Å)	2.81	3.30
R _{work} ^c (%)	24.03	22.69
R _{free} ^d (%)	29.98	25.67
Root-mean-square deviation		
Bonds (Å)	0.007	0.009
Angles (°)	1.4829	1.482
Average B factor (Å ²)	72.3	58.3
No. of atoms		
Protein	10,906	16,297
Ligand/ion	132	132
Water	73	0
B factors (Å²)		
Proteins	72.6	58.2
Ligand/ion	67.1	67.9
Water	42.9	0
Ramachandran plot (%)		
Preferred	97.46	97.85
Allowed	2.54	2.15
Outliers	0	0

Numbers in parentheses represent the values for the highest-resolution shell.

^aR_{merge} = $\sum |I_i - \langle I \rangle| / \sum I_i$, where I_i is the intensity of measured reflection and $\langle I \rangle$ is the mean intensity of all symmetry-related reflections.

^bCC_{1/2} was defined in (Karplus and Diederichs, 2012).

^cR_{work} = $\sum W ||F_{\text{calc}}| - |F_{\text{obs}}|| / \sum |F_{\text{obs}}|$, where F_{obs} and F_{calc} are observed and calculated structure factors. W is working dataset of about 95% of the total unique reflections randomly chosen and used for refinement.

^dR_{free} = $\sum_T ||F_{\text{calc}}| - |F_{\text{obs}}|| / \sum |F_{\text{obs}}|$, where T is a test dataset of about 5% of the total unique reflections randomly chosen and set aside before refinement.

of R12_{Shank3} significantly weakened the NTD/Rap1 interaction (Figures S3C–S3E). Correspondingly, the K22A mutant of Shank3 NTD-ANK interacted with Rap1 with a 1:1 stoichiometry and with a K_d of $\sim 3.4 \mu\text{M}$ (Figure 2E), which represents the

binding affinity of the second binding site of Shank3 NTD-ANK to Rap1.

There are two possible interfaces for the second Rap1 binding site on Shank3 NTD-ANK, which correspond to the two crystallographic symmetry-equivalent positions for Rap1 molecules (Figure S3F). The buried surface area of interface 1 (322 Å²) is much smaller than that of interface 2 (1,046 Å²) (Figure S3F). In addition, both “switch I” and “switch II” regions of Rap1 are involved in interface 2 (Figures 2A, 2B, 2D, and S3F), fitting with the biochemical data showing that only active Rap1 can directly interact with Shank3. In interface 1, neither switch I nor switch II is involved in the binding (Figure S3F). Thus, the interface 2 should be the second Rap1 binding site on Shank3 NTD-ANK, and interface 1 is the crystal-packing interface.

The C-terminal extension of ANK folds back to couple with the ANK domain through a series of hydrophobic interactions (Figure S4A). Three continuous, positively charged and highly conserved Arg residues (R355, R356, and R357; Figure S2) are involved in the coupling of the C-terminal extension to NTD-ANK (Figure S4A). A stretch of C-terminal residues of ANK also directly participate in the binding to Rap1 in the second binding site (Figure 2D). This stretch of residues were not resolved in the apo-form structure of Shank3 NTD-ANK presumably due to its undefined structure (Figure S4B). We purified a C-terminal truncated Shank3 NTD-ANK (residues 1–348, termed ΔCT in Figure 2E), which is exactly the same with the construct used in a previous study (Lilja et al., 2017). The Shank3 NTD-ANK ΔCT binds to Rap1 with a 1:1 stoichiometry and with a K_d of $\sim 0.85 \mu\text{M}$ (Figure 2E), indicating that the removal of part of the C-terminal extension of Shank3 NTD-ANK prevents Rap1 from binding to the second site of the tandem. The second binding site also contains two prominent pairs of salt bridges, K66_{Shank3}-D38_{Rap1} and R72_{Shank3}-E62_{Rap1}, which are in the vicinity of the switch I and switch II regions, respectively (Figure 2D). Substitution of either K66_{Shank3} or R72_{Shank3} with Glu completely eliminated Rap1's binding to the second site of Shank3 NTD-ANK, as either of the Shank3 mutants bound to Rap1 with a 1:1 stoichiometry and with a binding affinity comparable with the interaction between NTD and Rap1 (Figures S3B, S3G, and 2E). The residue corresponding to R72_{Shank3} is conserved in all Shank proteins (Figure S2), whereas the residue corresponding to K66_{Shank3} is only conserved in Shank2 and Shank3 (Figure S2). This analysis explains that Shank2, but not Shank1, also binds to Rap1 with a 1:2 stoichiometry (Figure 1B). Finally, a combination of the K22A and R72E mutations of Shank3 totally abolished the interaction between Shank3 and Rap1 (Figure 2E).

HRas Binds to Shank3 NTD-ANK with a Canonical Mode

Shank3 binds to HRas with a 1:1 stoichiometry and a much lower affinity than to Rap1 (Figure 1E). We speculated that HRas only binds to the first binding site of Shank3 NTD. We were not able to obtain crystals of the Shank3 NTD-ANK/HRas complex, so we sought to introduce mutations to Shank3 NTD based on the binding mode observed in the NTD/Rap1 interaction (Figure 2C) to stabilize Shank3 NTD-ANK/HRas complexes. The A42K mutation of Shank3 NTD-ANK was designed to introduce

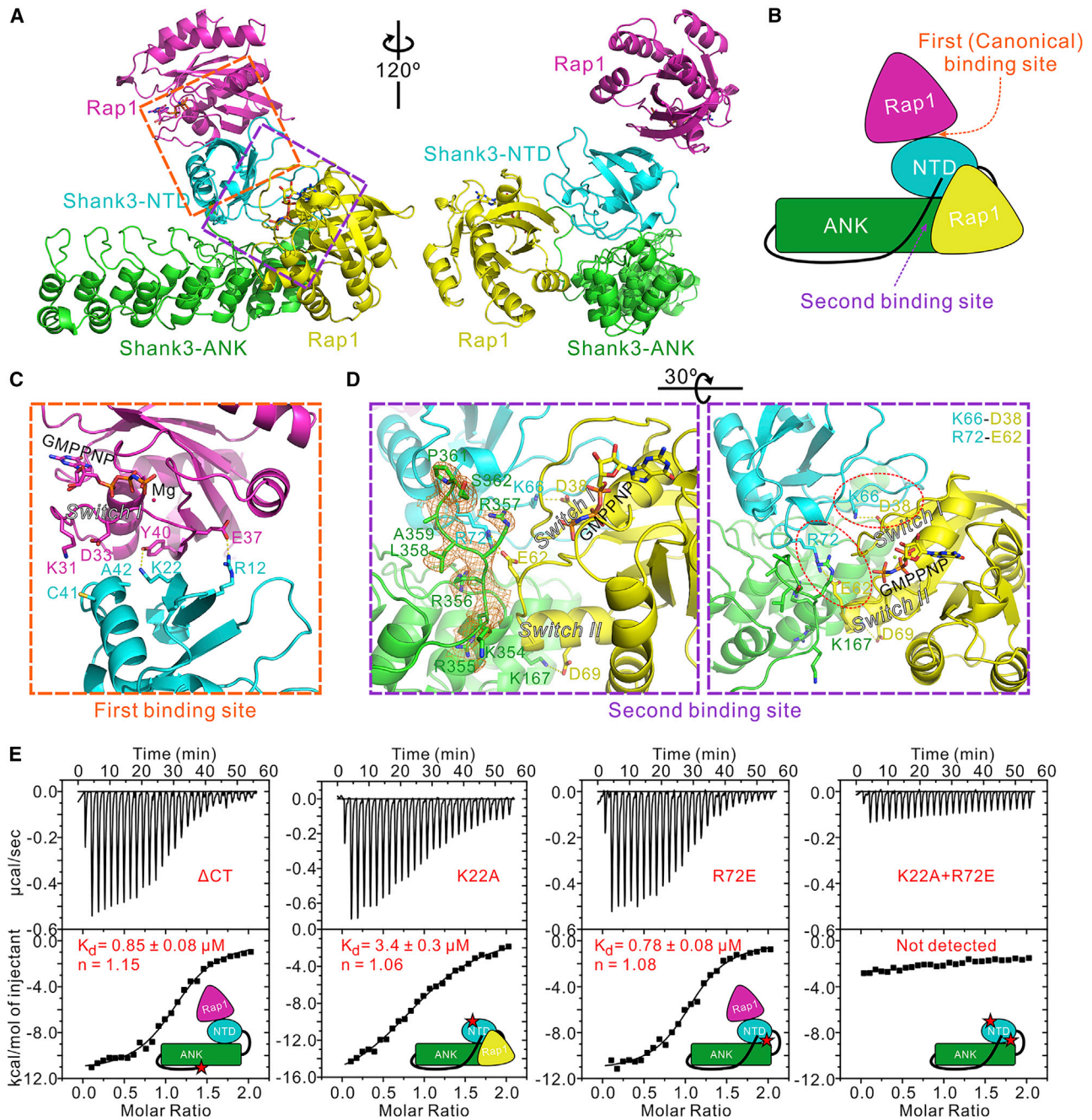


Figure 2. Structure of Shank3 NTD-ANK in Complex with GMPPNP-Bound Rap1

(A) Cartoon representation of the overall structure of Shank3 NTD-ANK in complex with GMPPNP-bound Rap1.

(B) Schematic diagram showing two distinct Rap1 binding sites of Shank3 NTD-ANK.

(C) The detailed interaction interface of the first (canonical) Rap1 binding site of Shank3.

(D) The detailed interaction interface of the second (unconventional) Rap1 binding site of Shank3. A $2mF_o - DF_c$ electron density map of the C-terminal tail of Shank3 NTD-ANK contoured at 1.0σ is represented as gold meshes.

(E) Interactions between Shank3 NTD-ANK mutants and GMPPNP-bound Rap1 measured by ITC. Shank3 NTD-ANK ($150\ \mu\text{M}$) in the syringe was titrated into $15\ \mu\text{M}$ GMPPNP-bound Rap1 in the cell.

See also Figures S2–S4.

a critical salt bridge with D33_{HRas}, and a C41K/A42K double mutant was used to introduce two pairs of salt bridges with E31_{HRas} and D33_{HRas} (Figure 2C). ITC-based binding experi-

ments showed that the A42K mutation could dramatically increase the binding affinity ($K_d \sim 0.88\ \mu\text{M}$, Figure S5A). Further substitution of Cys41 with Lys did not enhance the interaction

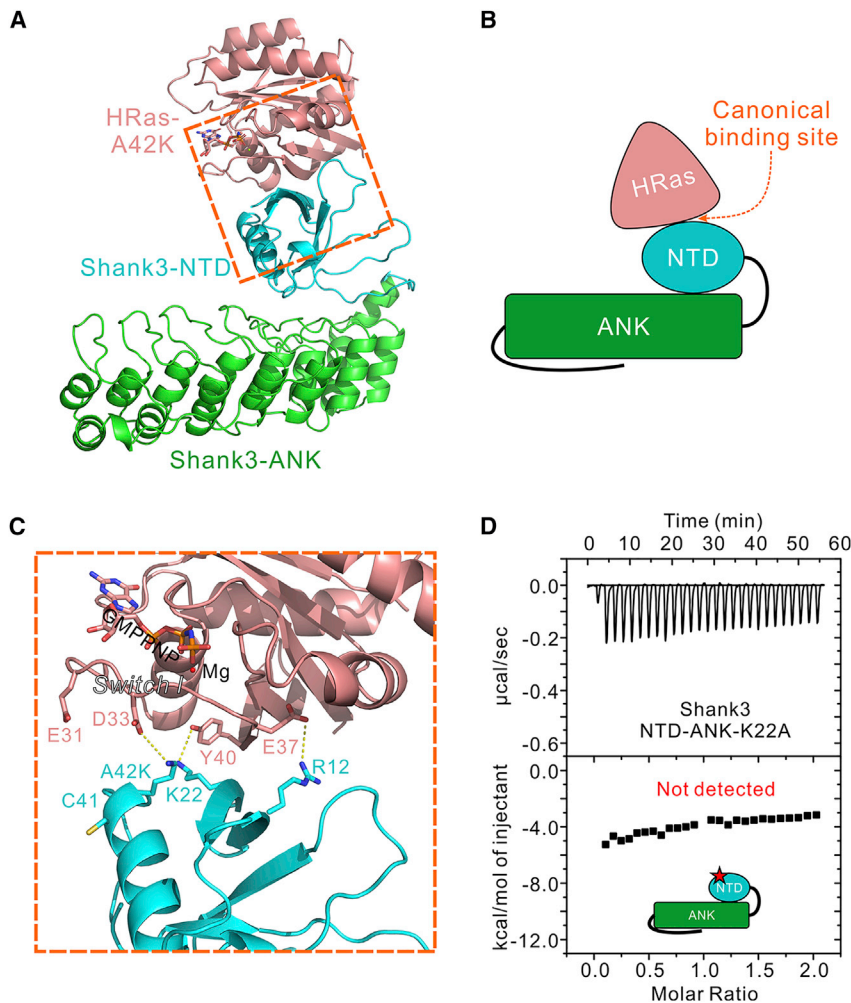


Figure 3. Structure of Shank3 NTD-ANK A42K Mutant in Complex with GMPPNP-Bound HRas

(A) Cartoon representation of the overall structure of Shank3 NTD-ANK A42K mutant in complex with GMPPNP-bound HRas. (B) Schematic diagram showing the canonical HRas binding site of Shank3 NTD-ANK. (C) The detailed interaction interface between Shank3 NTD-ANK and HRas. (D) Interaction between Shank3 NTD-ANK mutants and active HRas measured by ITC-based experiment. Shank3 NTD-ANK (150 μM) in the syringe was titrated into 15 μM GMPPNP-bound HRas in the cell. See also [Figures S2 and S5](#).

Shank3 Prevents SynGAP from Activating the GTPase Activity of Rap1

It has been reported that SynGAP predominantly activates Rap GTPase activity (Krapivinsky et al., 2004; Pena et al., 2008). We next investigated whether Shank3 might alter the SynGAP-mediated GTPase activation property of the Ras family enzymes. Consistent with previous reports, our *in vitro* GAP activity assay showed that SynGAP prominently stimulates the GTPase activity of Rap1 (Figure S6A). The structure of the Shank3 NTD-ANK in complex with GMPPNP-bound Rap1 revealed that the Shank3 NTD-ANK binding stabilizes the GTP-bound Rap1 conformation and should block SynGAP from binding to Rap1 (Figure S6B). Thus, binding of Shank3 to Rap1 might prevent SynGAP from stimulating

any further (Figure S5B). We were able to obtain crystals of Shank3 NTD-ANK A42K in complex with GMPPNP-bound HRas and determined the complex structure to the resolution of 3.30 \AA (Table 1).

The A42K mutant of Shank3 NTD-ANK binds to active HRas with a 1:1 stoichiometry and with a canonical binding mode (Figures 3A–3C). In addition to the canonical $\text{K22}_{\text{Shank3}}\text{-Y40}_{\text{HRas}}$ and $\text{R12}_{\text{Shank3}}\text{-E37}_{\text{HRas}}$ interactions, the mutation introduced, $\text{K42}_{\text{Shank3}}$, forms an additional electrostatic interaction with D33_{HRas} and thus enhances the binding affinity of the complex (Figure 3C). The wild-type (WT) Shank3 should have the same binding mode albeit with a lower affinity, as substitution of $\text{K22}_{\text{Shank3}}$ with Ala also abolished the Shank3 NTD-ANK and HRas interaction (Figure 3D). Curiously, HRas contains essentially all critical residues as those in Rap1 for binding to the second site of Shank3 NTD-ANK, but HRas does not bind to the second Rap1 binding site of Shank3 NTD-ANK. We do not have an explanation for this odd observation. As expected, neither the $\text{K66E}_{\text{Shank3}}$ nor the $\text{R72E}_{\text{Shank3}}$ mutants of Shank3 NTD-ANK had any impact on the binding of the tandem to HRas as the canonical binding site is totally separated from the second Rap1 binding site (Figures S5C and S5D).

the GTPase activity of Rap1. Indeed, addition of equimolar amounts of Shank3 NTD-ANK (e.g., 20 μM Shank3 NTD-ANK and 20 μM Rap1) near completely blocked the GTPase activity of Rap1 (Figure 4A). Addition of half-equivalent amounts of Shank3 NTD-ANK (e.g., 10 μM Shank3 and 20 μM Rap1) also greatly inhibited the GTPase activity of Rap1 (Figure 4A), because each Shank3 NTD-ANK has two Rap1 binding sites, and both can prevent SynGAP from stimulating the GTPase activity of Rap1. The K22A mutant (the canonical site 1 mutant) or the R72E mutant (the non-canonical site 2 mutant) of Shank3 NTD-ANK could still prevent SynGAP from stimulating the GTPase activity of Rap1, albeit requiring higher concentrations than the WT Shank3 NTD-ANK to reach the same level of inhibitions (Figures 4B and 4C). The K22A and R72E double mutant of Shank3 NTD-ANK is totally incapable of inhibiting SynGAP from activating Rap1 (Figure 4D), as the mutant has lost both Rap1 binding sites and has no detectable binding to Rap1 (Figure 2E). The apparent GTPase activities of the reaction mixtures are inversely proportional to the binding affinities of each form of Shank3 NTD-ANK to Rap1 (Figure 4E).

It is noted that Shank3 NTD-ANK binds to Rap1 with a moderately strong affinity (apparent $K_d \sim 0.47\text{--}0.84 \mu\text{M}$, Figure 1C), and blocks SynGAP from binding to Rap1 (Figure S6B). On the other hand, Rap1 effectors bind to Rap1 with moderately strong or

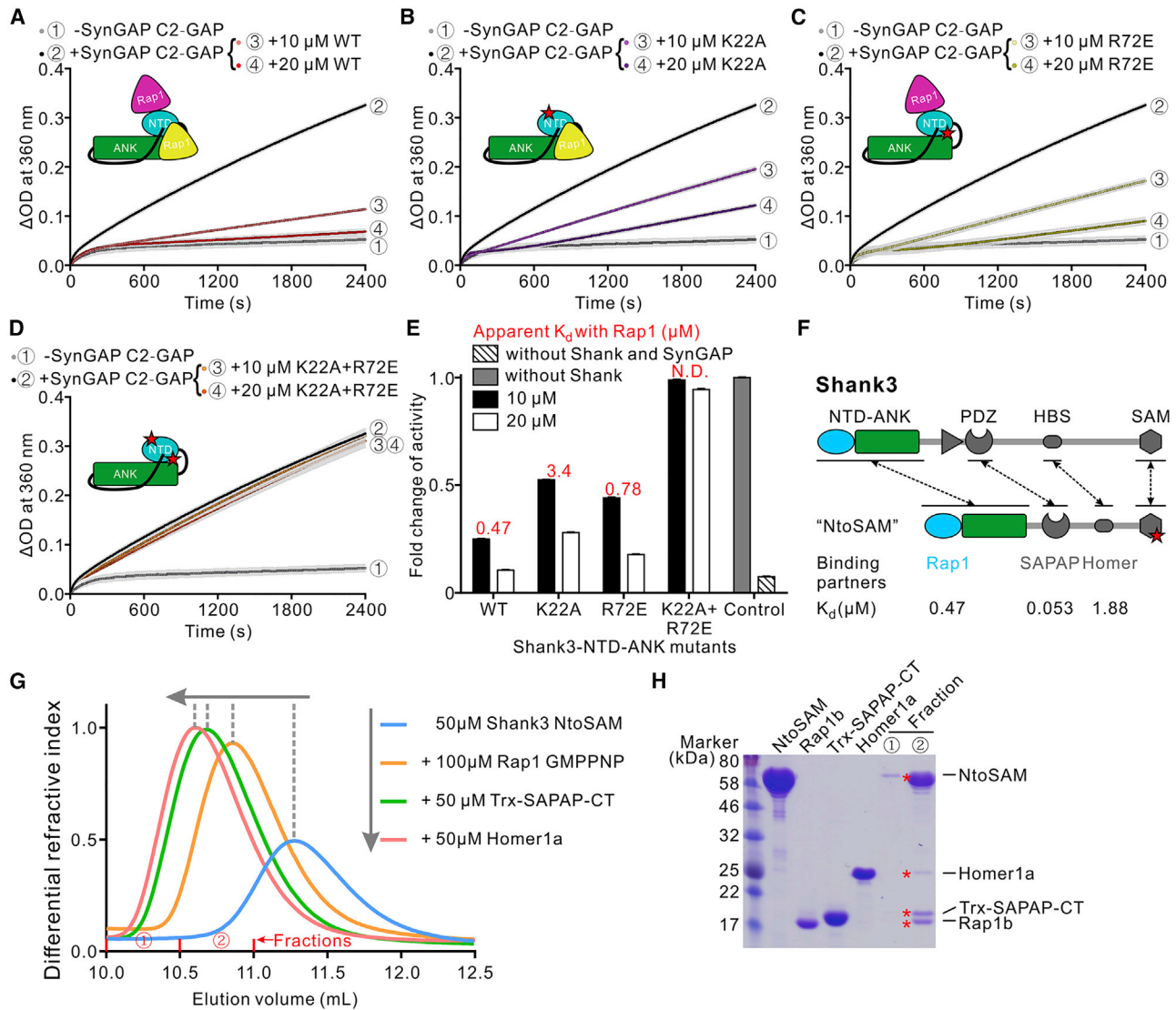


Figure 4. Shank3 Prevents SynGAP from Activating the GTPase Activity of Rap1

(A–D) *In vitro* GAP activity assays showing that binding of Shank3 to Rap1 sequesters Rap1 and prevent SynGAP from activating its GTPase activity (A). Mutations of the Rap1 binding sites can weaken or even abolish Shank3-mediated GTP hydrolysis inhibition of Rap1 (B–D). Control groups, including “–SynGAP C2-GAP” and “+SynGAP C2-GAP” groups as indicated in (A)–(D) are identical. Data represent three batches of independent experiments and are presented as mean \pm SD. (E) The fold GTPase activity reductions are inversely proportional to the binding affinities indicated in red color. Data are expressed as fold change \pm SE. (F) Schematic diagram showing the domain organization of Shank3 and the simplified version of “NtoSAM” used in the current study. The binding partners and their binding affinities are also indicated.

(G) Analytic gel filtration chromatography of Shank3 complex formation upon sequential additions of Shank3 binding partners.

(H) SDS-PAGE analysis showing that all binding partners were co-eluted with NtoSAM in the four-protein complex mixture.

See also Figure S6.

strong affinities (e.g., $K_d \sim 0.007 \mu\text{M}$ for the RaIGDS [Linnemann et al., 2002], $\sim 0.7 \mu\text{M}$ for the RIAM [Zhang et al., 2014], and $\sim 1.8 \mu\text{M}$ for the KRIT1 [Li et al., 2012]). Thus, the above GAP activity assays together with our structural analysis indicate that Shank3 can prevent SynGAP from activating GTPase activity of Rap1 by directly competing with SynGAP in binding to the active form of Rap1. By doing so, Shank3 may be able to protect the active form of Rap1 from SynGAP-mediated inactivation before acting on its effectors.

Rap1 Can Be Incorporated into a Shank-Mediated Protein-Protein Interaction Network in PSDs

We next studied whether Rap1 can be incorporated into Shank3-organized PSD protein complexes. We were not able to prepare full-length recombinant Shank proteins likely due to their large sizes. Based on our previously reported, simplified Shank3 [Zeng et al., 2018], we further added the NTD-ANK tandem and generated an updated version of simplified Shank3 (termed NtoSAM, Figure 4F). NtoSAM consists of an NTD-ANK tandem,

an extended PDZ domain specifically binding to a SAPAP tail (Zeng et al., 2016), a Homer-binding sequence and a C-terminal SAM domain with M1718E mutation to improve protein solubility (Baron et al., 2006) (Figure 4F). The version of Shank3 used in the current study lacks most of the low complexity and predicted unstructured regions between these domains.

Using analytical gel filtration chromatography, we monitored the complex formation by adding three Shank3 binding partners one by one: first Rap1, then the C-terminal tail of SAPAP (termed SAPAP-CT), and finally Homer1a. The analytic gel filtration chromatographic experiments showed that the elution volumes of the mixtures were progressively shifting to smaller volumes upon mixing one (Rap1), or two (Rap1 and SAPAP-CT), or all three (Rap1, SAPAP-CT, and Homer1a) proteins with Shank3 NtoSAM (Figure 4G), indicating that all three target proteins can simultaneously bind to Shank3. SDS-PAGE analysis of the four-protein mixture showed that all binding partners were co-eluted with NtoSAM on gel filtration chromatography (Figure 4H), demonstrating that Rap1 can be incorporated into Shank-mediated PSD protein interaction network.

LTP Induction Promotes Shank3 Binding to Ras Superfamily Proteins in Postsynaptic Density

We hypothesized that the interactions between Shank proteins and Ras superfamily proteins in dendritic spine might be modulated by synaptic plasticity. Under resting condition, SynGAP is highly enriched in dendritic spines to keep Ras superfamily proteins majorly in GDP form. Thus, there is little interaction between Shank and Ras superfamily proteins. LTP induction triggers dispersion of SynGAP (Araki et al., 2015), which would shift Ras superfamily proteins to the GTP-bound active form that is favorable for binding to Shank.

Thus we sought to investigate whether Shank3 could interact with HRas or Rap1 at the single spine level upon LTP induction. We monitored Shank3 and HRas or Rap1 interaction in dendritic spines of CA1 pyramidal neurons in hippocampal organotypic slice cultures using Förster resonance energy transfer-fluorescence lifetime imaging microscopy (FRET-FLIM) method (Saneyoshi et al., 2019). N-terminal enhanced GFP-tagged Shank3 and N-terminal mCherry-tagged HRas or Rap1 were co-transfected into neurons (Figure 5A). Several mutations of Shank3 identified from our biochemical experiments (the K22A and R72E single mutants and the K22A/R72E double mutant) were also investigated in the FRET-FLIM experiments. We stimulated single dendritic spine with a protocol that typically induce structural LTP (Saneyoshi et al., 2019). However, overexpression of Shank3 in neurons induces spine enlargements (Sala et al., 2001) and further stimulation of synapse with glutamate uncaging do not induce additional enlargement of spines. Nevertheless, there was a dramatic increase in FRET following the LTP-inducing stimulation with glutamate uncaging in the WT Shank3- and HRas-expressing neurons that persisted at least 15 min after the stimulation, indicating that Shank3 and HRas interacted with each other persistently (Figures 5B and 5C). Neither the K22A mutant nor the K22/R72E double mutant of Shank3 showed detectable LTP-induced binding to HRas (Figures 5B and 5C), as neither mutant is capable of binding to Ras proteins (Figure 3D). In contrast, the R72E mutant of Shank3 showed significant interaction

with HRas (Figures 5B and 5C), as R72 is in the second Rap1 binding site and the R72E mutation does not affect Shank3's binding to HRas (Figures 2 and S3H).

For Shank3 WT and Rap1, the induction of LTP also significantly triggered their interaction. Surprisingly, unlike HRas, the interaction between Shank3 and Rap1 was transient and the change of fluorescence lifetime quickly went back to the baseline (Figures 5D and 5E), suggesting different regulation mechanisms for Rap1 and HRas to dissociate from Shank3 in dendritic spines. Interestingly, neither the K22A mutant nor the R72E mutant could undergo LTP-induced binding to Rap1, indicating that both binding sites on the NTD-ANK tandem are required for Rap1 to bind to Shank3 in dendritic spines of living neurons (Figures 5D and 5E). As expected, the K22A/R72E double mutation of Shank3 showed no LTP-induced binding to Rap1 (Figures 5D and 5E).

Taken together, the interactions between Shank3 and HRas or Rap1 can be triggered by LTP induction. Although HRas and Rap1 show high amino acid sequence identity and share a similar Ras-association domain-mediated binding mode, HRas binding to Shank3 is long-lasting and Rap1 binding to Shank3 is transient. The distinct Shank3 binding kinetics for HRas and Rap1 may be correlated to different roles played by HRas and Rap1 in synaptic plasticity (Zhu et al., 2002).

DISCUSSION

In this study, we discovered that Rap1 and HRas, two conserved members of Ras superfamily, interact with the Shank NTD-ANK tandem with distinct binding modes. Rap1 interacts with Shank2 or Shank3 with a 2:1 stoichiometry, whereas HRas binds to Shank proteins with a 1:1 stoichiometry. Our crystal structures further revealed that Rap1, in addition to the canonical Ras-association domain (or NTD) binding site as predicted previously (Lilja et al., 2017), uses an unconventional binding site formed by both NTD and ANK of Shank3. Both Rap1 binding sites of Shank3 directly involve the specific conformations of switch I and switch II regions of the GTP-bound form of Rap1, explaining that only active (GTP bound) Ras proteins can bind to Shank.

Rap was initially identified as an antagonist of Ras (Cook et al., 1993; Kitayama et al., 1989), because Rap and HRas have high amino acid identity, and share many binding partners. Rap was then discovered to be involved in signaling pathways distinct from Ras and has its own specific effectors (Bos, 1998; Ohtsuka et al., 1996). In synapse, Ras and Rap mediate independent signaling pathways in activity-dependent synaptic plasticity (Zhang et al., 2018; Zhu et al., 2002). The distinct binding modes of Shank3 to Rap1 and HRas may contribute to their specific downstream signaling pathways.

We provided evidence that the interactions between Shank proteins and Ras superfamily proteins in dendritic spine are modulated by synaptic plasticity. Small GTPases usually are modulated by molecular switches during synaptic plasticity. LTP induction will “turn on” the molecular switches to convert small GTPases to GTP-bound form for Shank binding. Thus the interaction between Shank and Ras superfamily proteins are initiated by LTP induction. On the other hand, LTP needs a mechanism to convert short Ca^{2+} pulses into long-lasting

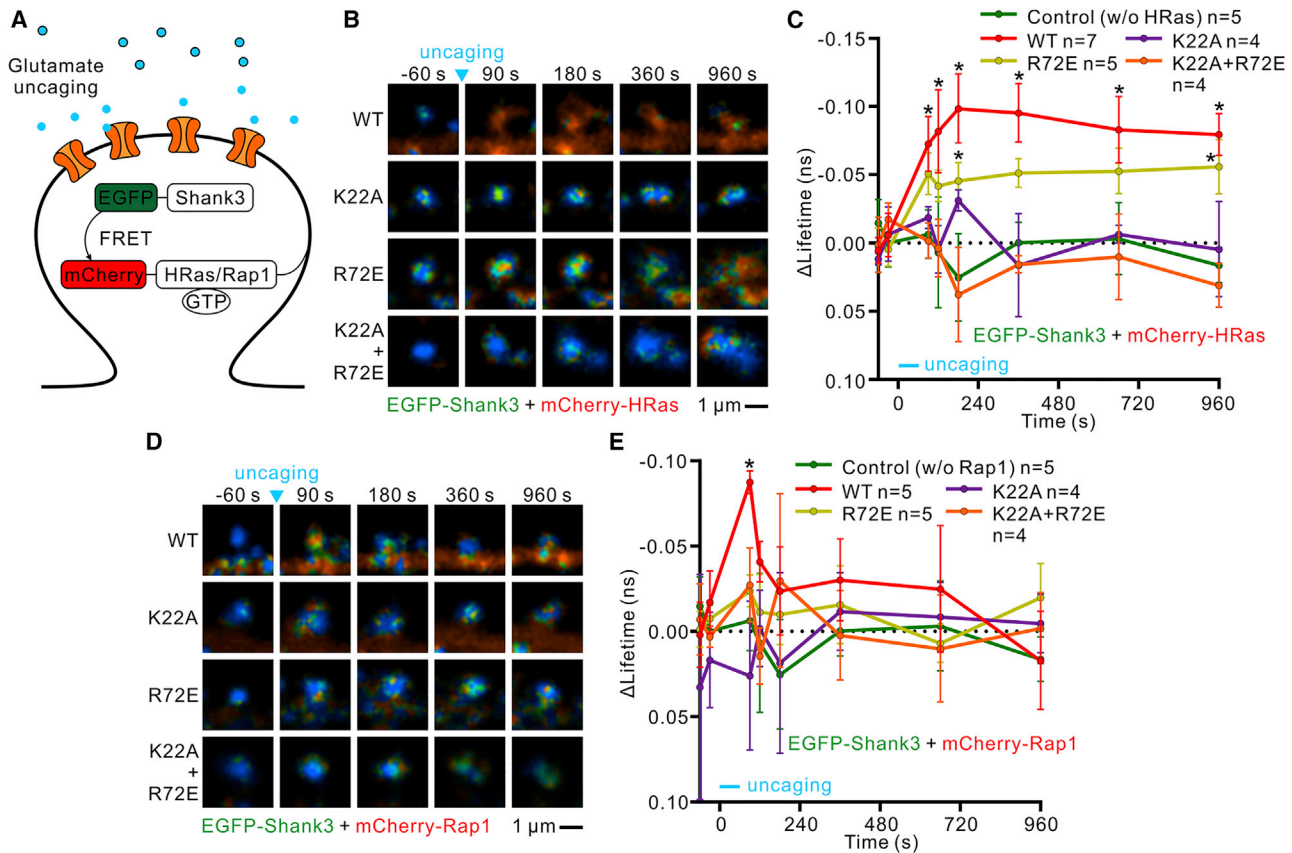


Figure 5. LTP Induction Promotes Shank3 and Ras Superfamily Proteins Interaction in Postsynaptic Density

(A) Schematic diagram showing experimental design of FRET-FLIM. N-terminal EGFP-tagged Shank3 as donor and N-terminal mCherry-tagged Rap1 or HRas as acceptor were co-transfected into hippocampal neurons. Single spine was stimulated by uncaging MNI-glutamate using a two-photon laser.

(B) Interaction between various forms of Shank3 and HRas as visualized by FRET-FLIM before and after glutamate uncaging. Warmer color hues indicate more interaction.

(C) Averaged time course of the interactions between various forms of Shank3 and HRas measured as a change of the lifetime of EGFP-Shank3 after glutamate uncaging. Data are expressed as the mean \pm SEM.

(D) Interaction between various forms of Shank3 and Rap1 as visualized by FRET-FLIM before and after glutamate uncaging.

(E) Averaged time course of the interactions between various forms of Shank3 and Rap1 measured as a change of the lifetime of EGFP-Shank3 after glutamate uncaging. Data are expressed as the mean \pm SEM.

Numbers of observation (n) indicated in (C and E) represent the number of spines that were imaged, and one spine was selected from one neuron for each assay.

* $p < 0.05$, compared with a control group in which only EGFP-Shank3 was transfected using one-way ANOVA with Scheffé's post hoc comparison. Control group presented in (C and E) are identical. Because both groups were tested at the same time, we pooled control groups together.

structural and functional plasticity. Recently, the formation of reciprocally activating signaling complex between CaMKII and a small GTPase modulator, TIAM1, was reported to be responsible for maintaining the enlargement of dendritic spines during LTP (Saneyoshi et al., 2019). Here, our biochemical data suggest that Shank can compete with SynGAP for HRas/Rap1, and thus slow down GTP hydrolysis for HRas/Rap1. This will induce a sustained interaction between Shank and small GTPases, which may be a potential mechanism for storing the active form of small GTPases for the following long-lasting structural and functional LTP.

Our structural data revealed two distinct Rap1 binding sites on Shank3 with an order of magnitude differences in affinities ($K_d \sim 0.41 \mu\text{M}$ for site 1 and $K_d \sim 3.4 \mu\text{M}$ for site 2). Considering that Shank is one of the most abundant scaffolding protein in PSDs, highly compartmentalized and abundant Shank proteins

can potentially recruit and "store" an active form of small GTPases in PSDs for its downstream signaling events. Two distinct Rap1 binding sites on Shank3 provide a potential mechanism for the fine-tune of Rap1 signaling pathway. For the Rap1 effectors with much lower binding affinities, Shank3 can function as a "barrier" to limit the weak effectors from accessing Rap1. For the Rap1 effectors with modest affinities, only part of Rap1, which binds to the second site, may be preferentially released to be accessible by the modest effectors. For the strong effectors, Rap1 bound to both sites on Shank3 would be released for binding to the strong effectors. At same time, Shank3 itself may be an effector of Rap1/HRas, but the hypothesis needs to be investigated in the future. Our FRET-FLIM data also suggest a distinct dissociation mechanism of Rap1 from the Shank scaffold in neuronal spines after LTP stimulation.

STAR★METHODS

Detailed methods are provided in the online version of this paper and include the following:

- KEY RESOURCES TABLE
- LEAD CONTACT AND MATERIALS AVAILABILITY
- EXPERIMENTAL MODEL AND SUBJECT DETAILS
 - Animals
 - Bacterial Strain
- METHODS DETAILS
 - Constructs
 - Protein Expression and Purification
 - Protein Crystallization and Structure Determination
 - Isothermal Titration Calorimetry (ITC) Assay
 - GAP Activity Assay
 - Glutamate Uncaging and Fluorescent Lifetime Imaging
- QUANTIFICATION AND STATISTICAL ANALYSIS
- DATA AND CODE AVAILABILITY

SUPPLEMENTAL INFORMATION

Supplemental Information can be found online at <https://doi.org/10.1016/j.str.2019.11.018>.

ACKNOWLEDGMENTS

We thank the BL19U1 beamline at National Facility for Protein Science Shanghai (NFPS) and BL17U1 beamline at Shanghai Synchrotron Radiation Facility (SSRF) for X-ray beam time. This work was supported by grants from the Simons Foundation (Award ID: 510178) and RGC of Hong Kong (AoE-M09-12) to M.Zhang, and MEXT, Japan (18H05434 to Y.H.; 17K14947 and 18KK0421 to T.H.), and The Takeda Science Foundation (to Y.H.), and Narishige Neuroscience Research Foundation (to T.H.), and Research Foundation for Opto-Science and Technology (to T.H.), and SPRIRITS Kyoto University (to Y.H. and T.H.), and an HFSP Research Grant (RGP0020/2019 to Y.H. and M.Zhang). M.Zhang is a Kerry Holdings Professor in Science and a Senior Fellow of IAS at HKUST.

AUTHOR CONTRIBUTIONS

Q.C., T.H., and M.Zeng performed the experiments. Q.C., T.H., M.Zeng, Y.H., and M.Zhang analyzed the data. Q.C., T.H., and M.Zhang designed the research. Q.C. and M.Zhang drafted the paper and all authors commented on the paper, and M.Zhang coordinated the project.

DECLARATION OF INTERESTS

The authors declare no competing interests.

Received: September 22, 2019

Revised: October 31, 2019

Accepted: November 27, 2019

Published: December 23, 2019

REFERENCES

- Araki, Y., Zeng, M., Zhang, M., and Haganir, R.L. (2015). Rapid dispersion of SynGAP from synaptic spines triggers AMPA receptor insertion and spine enlargement during LTP. *Neuron* 85, 173–189.
- Baron, M.K., Boeckers, T.M., Vaida, B., Faham, S., Gingery, M., Sawaya, M.R., Salyer, D., Gundelfinger, E.D., and Bowie, J.U. (2006). An architectural framework that may lie at the core of the postsynaptic density. *Science* 311, 531–535.
- Bockers, T.M., Mameza, M.G., Kreutz, M.R., Bockmann, J., Weise, C., Buck, F., Richter, D., Gundelfinger, E.D., and Kreienkamp, H.J. (2001). Synaptic scaffolding proteins in rat brain. Ankyrin repeats of the multidomain Shank protein family interact with the cytoskeletal protein alpha-fodrin. *J. Biol. Chem.* 276, 40104–40112.
- Bonaglia, M.C., Giorda, R., Mani, E., Aceti, G., Anderlid, B.M., Baroncini, A., Pramparo, T., and Zuffardi, O. (2006). Identification of a recurrent breakpoint within the SHANK3 gene in the 22q13.3 deletion syndrome. *J. Med. Genet.* 43, 822–828.
- Bos, J.L. (1998). All in the family? New insights and questions regarding interconnectivity of Ras, Rap1 and Ral. *EMBO J.* 17, 6776–6782.
- Bosch, M., Castro, J., Saneyoshi, T., Matsuno, H., Sur, M., and Hayashi, Y. (2014). Structural and molecular remodeling of dendritic spine substructures during long-term potentiation. *Neuron* 82, 444–459.
- Chen, V.B., Arendall, W.B., 3rd, Headd, J.J., Keedy, D.A., Immormino, R.M., Kapral, G.J., Murray, L.W., Richardson, J.S., and Richardson, D.C. (2010). MolProbity: all-atom structure validation for macromolecular crystallography. *Acta Crystallogr. D Biol. Crystallogr.* 66, 12–21.
- Cook, S.J., Rubinfeld, B., Albert, I., and McCormick, F. (1993). RapV12 antagonizes Ras-dependent activation of ERK1 and ERK2 by LPA and EGF in Rat-1 fibroblasts. *EMBO J.* 12, 3475–3485.
- Durand, C.M., Betancur, C., Boeckers, T.M., Bockmann, J., Chaste, P., Fauchereau, F., Nygren, G., Rastam, M., Gillberg, I.C., Anckarsater, H., et al. (2007). Mutations in the gene encoding the synaptic scaffolding protein SHANK3 are associated with autism spectrum disorders. *Nat. Genet.* 39, 25–27.
- Emsley, P., Lohkamp, B., Scott, W.G., and Cowtan, K. (2010). Features and development of Coot. *Acta Crystallogr. D Biol. Crystallogr.* 66, 486–501.
- Gauthier, J., Spiegelman, D., Piton, A., Lafreniere, R.G., Laurent, S., St-Onge, J., Lapointe, L., Hamdan, F.F., Cossette, P., Mottron, L., et al. (2009). Novel de novo SHANK3 mutation in autistic patients. *Am. J. Med. Genet. B Neuropsychiatr. Genet.* 150B, 421–424.
- Han, K., Holder, J.L., Jr., Schaaf, C.P., Lu, H., Chen, H., Kang, H., Tang, J., Wu, Z., Hao, S., Cheung, S.W., et al. (2013). SHANK3 overexpression causes manic-like behaviour with unique pharmacogenetic properties. *Nature* 503, 72–77.
- Harvey, C.D., Yasuda, R., Zhong, H., and Svoboda, K. (2008). The spread of Ras activity triggered by activation of a single dendritic spine. *Science* 321, 136–140.
- Hayashi, M.K., Tang, C., Verpelli, C., Narayanan, R., Stearns, M.H., Xu, R.M., Li, H., Sala, C., and Hayashi, Y. (2009). The postsynaptic density proteins Homer and Shank form a polymeric network structure. *Cell* 137, 159–171.
- Hedrick, N.G., Harward, S.C., Hall, C.E., Murakoshi, H., McNamara, J.O., and Yasuda, R. (2016). Rho GTPase complementation underlies BDNF-dependent homo- and heterosynaptic plasticity. *Nature* 538, 104–108.
- Huang, L., Hofer, F., Martin, G.S., and Kim, S.H. (1998). Structural basis for the interaction of ras with RalGDS. *Nat. Struct. Biol.* 5, 422–426.
- Jiang, Y.H., and Ehlers, M.D. (2013). Modeling autism by SHANK gene mutations in mice. *Neuron* 78, 8–27.
- John, J., Sohmen, R., Feuerstein, J., Linke, R., Wittinghofer, A., and Goody, R.S. (1990). Kinetics of interaction of nucleotides with nucleotide-free H-ras p21. *Biochemistry* 29, 6058–6065.
- Karplus, P.A., and Diederichs, K. (2012). Linking crystallographic model and data quality. *Science* 336, 1030–1033.
- Kim, E., and Sheng, M. (2004). PDZ domain proteins of synapses. *Nat. Rev. Neurosci.* 5, 771–781.
- Kim, J.H., Lee, H.K., Takamiya, K., and Haganir, R.L. (2003). The role of synaptic GTPase-activating protein in neuronal development and synaptic plasticity. *J. Neurosci.* 23, 1119–1124.
- Kitayama, H., Sugimoto, Y., Matsuzaki, T., Ikawa, Y., and Noda, M. (1989). A ras-related gene with transformation suppressor activity. *Cell* 56, 77–84.
- Komiyama, N.H., Watabe, A.M., Carlisle, H.J., Porter, K., Charlesworth, P., Monti, J., Strathdee, D.J., O'Carroll, C.M., Martin, S.J., Morris, R.G., et al. (2002). SynGAP regulates ERK/MAPK signaling, synaptic plasticity, and

- learning in the complex with postsynaptic density 95 and NMDA receptor. *J. Neurosci.* **22**, 9721–9732.
- Krapivinsky, G., Medina, I., Krapivinsky, L., Gapon, S., and Clapham, D.E. (2004). SynGAP-MUPP1-CaMKII synaptic complexes regulate p38 MAP kinase activity and NMDA receptor-dependent synaptic AMPA receptor potentiation. *Neuron* **43**, 563–574.
- Leblond, C.S., Nava, C., Polge, A., Gauthier, J., Huguet, G., Lumbroso, S., Giuliano, F., Stordeur, C., Depienne, C., Mouzat, K., et al. (2014). Meta-analysis of SHANK mutations in autism spectrum disorders: a gradient of severity in cognitive impairments. *PLoS Genet.* **10**, e1004580.
- Li, X., Zhang, R., Draheim, K.M., Liu, W., Calderwood, D.A., and Boggon, T.J. (2012). Structural basis for small G protein effector interaction of Ras-related protein 1 (Rap1) and adaptor protein Krev interaction trapped 1 (KRIT1). *J. Biol. Chem.* **287**, 22317–22327.
- Lilja, J., Zacharchenko, T., Georgiadou, M., Jacquemet, G., De Franceschi, N., Peuhu, E., Hamidi, H., Pouwels, J., Martens, V., Nia, F.H., et al. (2017). SHANK proteins limit integrin activation by directly interacting with Rap1 and R-Ras. *Nat. Cell Biol.* **19**, 292–305.
- Lim, S., Sala, C., Yoon, J., Park, S., Kuroda, S., Sheng, M., and Kim, E. (2001). Sharpin, a novel postsynaptic density protein that directly interacts with the shank family of proteins. *Mol. Cell. Neurosci.* **17**, 385–397.
- Linnemann, T., Kiel, C., Herter, P., and Hermann, C. (2002). The activation of RalGDS can be achieved independently of its Ras binding domain. Implications of an activation mechanism in Ras effector specificity and signal distribution. *J. Biol. Chem.* **277**, 7831–7837.
- Mameza, M.G., Dvoretzkova, E., Bamann, M., Honck, H.H., Guler, T., Boeckers, T.M., Schoen, M., Verpelli, C., Sala, C., Barsukov, I., et al. (2013). SHANK3 gene mutations associated with autism facilitate ligand binding to the Shank3 ankyrin repeat region. *J. Biol. Chem.* **288**, 26697–26708.
- McCoy, A.J., Grosse-Kunstleve, R.W., Adams, P.D., Winn, M.D., Storoni, L.C., and Read, R.J. (2007). Phaser crystallographic software. *J. Appl. Crystallogr.* **40**, 658–674.
- Moessner, R., Marshall, C.R., Sutcliffe, J.S., Skaug, J., Pinto, D., Vincent, J., Zwaigenbaum, L., Fernandez, B., Roberts, W., Szatmari, P., et al. (2007). Contribution of SHANK3 mutations to autism spectrum disorder. *Am. J. Hum. Genet.* **81**, 1289–1297.
- Monteiro, P., and Feng, G. (2017). SHANK proteins: roles at the synapse and in autism spectrum disorder. *Nat. Rev. Neurosci.* **18**, 147–157.
- Murakoshi, H., Wang, H., and Yasuda, R. (2011). Local, persistent activation of Rho GTPases during plasticity of single dendritic spines. *Nature* **472**, 100–104.
- Murshudov, G.N., Skubak, P., Lebedev, A.A., Pannu, N.S., Steiner, R.A., Nicholls, R.A., Winn, M.D., Long, F., and Vagin, A.A. (2011). REFMAC5 for the refinement of macromolecular crystal structures. *Acta Crystallogr. D Biol. Crystallogr.* **67**, 355–367.
- Naisbitt, S., Kim, E., Tu, J.C., Xiao, B., Sala, C., Valtschanoff, J., Weinberg, R.J., Worley, P.F., and Sheng, M. (1999). Shank, a novel family of postsynaptic density proteins that binds to the NMDA receptor/PSD-95/GKAP complex and cortactin. *Neuron* **23**, 569–582.
- Nassar, N., Horn, G., Herrmann, C., Scherer, A., McCormick, F., and Wittinghofer, A. (1995). The 2.2 Å crystal structure of the Ras-binding domain of the serine/threonine kinase c-Raf1 in complex with Rap1A and a GTP analogue. *Nature* **375**, 554–560.
- Nassar, N., Horn, G., Herrmann, C., Block, C., Janknecht, R., and Wittinghofer, A. (1996). Ras/Rap effector specificity determined by charge reversal. *Nat. Struct. Biol.* **3**, 723–729.
- Ohtsuka, T., Shimizu, K., Yamamori, B., Kuroda, S., and Takai, Y. (1996). Activation of brain B-Raf protein kinase by Rap1B small GTP-binding protein. *J. Biol. Chem.* **271**, 1258–1261.
- Otwinowski, Z., and Minor, W. (1997). Processing of X-ray diffraction data collected in oscillation mode. *Methods Enzymol.* **276**, 307–326.
- Peca, J., Feliciano, C., Ting, J.T., Wang, W., Wells, M.F., Venkatraman, T.N., Lascola, C.D., Fu, Z., and Feng, G. (2011). Shank3 mutant mice display autistic-like behaviours and striatal dysfunction. *Nature* **472**, 437–442.
- Pena, V., Hothorn, M., Eberth, A., Kaschau, N., Parret, A., Gremer, L., Bonneau, F., Ahmadian, M.R., and Scheffzek, K. (2008). The C2 domain of SynGAP is essential for stimulation of the Rap GTPase reaction. *EMBO Rep.* **9**, 350–355.
- Sala, C., Piech, V., Wilson, N.R., Passafaro, M., Liu, G., and Sheng, M. (2001). Regulation of dendritic spine morphology and synaptic function by Shank and Homer. *Neuron* **31**, 115–130.
- Sala, C., Vicidomini, C., Bigi, I., Mossa, A., and Verpelli, C. (2015). Shank synaptic scaffold proteins: keys to understanding the pathogenesis of autism and other synaptic disorders. *J. Neurochem.* **135**, 849–858.
- Saneyoshi, T., Matsuno, H., Suzuki, A., Murakoshi, H., Hedrick, N.G., Agnello, E., O’Connell, R., Stratton, M.M., Yasuda, R., and Hayashi, Y. (2019). Reciprocal activation within a kinase-effector complex underlying persistence of structural LTP. *Neuron* **102**, 1199–1210.e6.
- Schmeisser, M.J., Ey, E., Wegener, S., Bockmann, J., Stempel, A.V., Kuebler, A., Janssen, A.L., Udvardi, P.T., Shibani, E., Spilker, C., et al. (2012). Autistic-like behaviours and hyperactivity in mice lacking ProSAP1/Shank2. *Nature* **486**, 256–260.
- Sheng, M., and Hoogenraad, C.C. (2007). The postsynaptic architecture of excitatory synapses: a more quantitative view. *Annu. Rev. Biochem.* **76**, 823–847.
- Ting, J.T., Peca, J., and Feng, G. (2012). Functional consequences of mutations in postsynaptic scaffolding proteins and relevance to psychiatric disorders. *Annu. Rev. Neurosci.* **35**, 49–71.
- Tu, J.C., Xiao, B., Naisbitt, S., Yuan, J.P., Petralia, R.S., Brakeman, P., Doan, A., Aakalu, V.K., Lanahan, A.A., Sheng, M., et al. (1999). Coupling of mGluR/Homer and PSD-95 complexes by the Shank family of postsynaptic density proteins. *Neuron* **23**, 583–592.
- Won, H., Lee, H.R., Gee, H.Y., Mah, W., Kim, J.I., Lee, J., Ha, S., Chung, C., Jung, E.S., Cho, Y.S., et al. (2012). Autistic-like social behaviour in Shank2-mutant mice improved by restoring NMDA receptor function. *Nature* **486**, 261–265.
- Yi, F., Danko, T., Botelho, S.C., Patzke, C., Pak, C., Wernig, M., and Sudhof, T.C. (2016). Autism-associated SHANK3 haploinsufficiency causes Ih channelopathy in human neurons. *Science* **352**, aaf2669.
- Zeng, M., Shang, Y., Guo, T., He, Q., Yung, W.H., Liu, K., and Zhang, M. (2016). A binding site outside the canonical PDZ domain determines the specific interaction between Shank and SAPAP and their function. *Proc. Natl. Acad. Sci. U S A* **113**, E3081–E3090.
- Zeng, M., Chen, X., Guan, D., Xu, J., Wu, H., Tong, P., and Zhang, M. (2018). Reconstituted postsynaptic density as a molecular platform for understanding synapse formation and plasticity. *Cell* **174**, 1172–1187.e16.
- Zhang, H., Chang, Y.C., Brennan, M.L., and Wu, J. (2014). The structure of Rap1 in complex with RIAM reveals specificity determinants and recruitment mechanism. *J. Mol. Cell Biol.* **6**, 128–139.
- Zhang, L., Zhang, P., Wang, G., Zhang, H., Zhang, Y., Yu, Y., Zhang, M., Xiao, J., Crespo, P., Hell, J.W., et al. (2018). Ras and Rap signal bidirectional synaptic plasticity via distinct subcellular microdomains. *Neuron* **98**, 783–800.e4.
- Zhou, Y., Sharma, J., Ke, Q., Landman, R., Yuan, J., Chen, H., Hayden, D.S., Fisher, J.W., 3rd, Jiang, M., Menegas, W., et al. (2019). Atypical behaviour and connectivity in SHANK3-mutant macaques. *Nature* **570**, 326–331.
- Zhu, J.J., Qin, Y., Zhao, M., Van Aelst, L., and Malinow, R. (2002). Ras and Rap control AMPA receptor trafficking during synaptic plasticity. *Cell* **110**, 443–455.
- Zhu, J., Shang, Y., and Zhang, M. (2016). Mechanistic basis of MAGUK-organized complexes in synaptic development and signalling. *Nat. Rev. Neurosci.* **17**, 209–223.

STAR★METHODS

KEY RESOURCES TABLE

REAGENT or RESOURCE	SOURCE	IDENTIFIER
Chemicals, Peptides, and Recombinant Proteins		
Chemicals: Tetrodotoxin	Latoxan laboratory	Cat#L8503
Chemicals: Picrotoxin	Nacalai tesque	Cat#28004-71
Chemicals: MNI-caged-L-glutamate	Tocris	Cat#1490
Chemicals: EnzChek phosphate assay kit	ThermoFisher	Cat#E6646
Recombinant protein: Shank1-NTD-ANK (aa 73-440)	This paper	N/A (custom-made)
Recombinant protein: Shank2-NTD-ANK (aa 49-423)	This paper	N/A (custom-made)
Recombinant protein: Shank3-NTD-ANK (aa 1-376)	This paper	N/A (custom-made)
Recombinant protein: Shank3-NTD-ANK (aa 1-368)	This paper	N/A (custom-made)
Recombinant protein: Shank3-NTD-ANK (aa 1-362)	This paper	N/A (custom-made)
Recombinant protein: Shank3-NTD-ANK-A42K (aa 1-362)	This paper	N/A (custom-made)
Recombinant protein: Shank3-NTD-ANK-C41K+A42K (aa 1-362)	This paper	N/A (custom-made)
Recombinant protein: Shank3-NTD-ANK-ΔCT (aa 1-348)	This paper	N/A (custom-made)
Recombinant protein: Shank3-NTD-ANK-K22A (aa 1-376)	This paper	N/A (custom-made)
Recombinant protein: Shank3-NTD-ANK-K66E (aa 1-376)	This paper	N/A (custom-made)
Recombinant protein: Shank3-NTD-ANK-R72E (aa 1-376)	This paper	N/A (custom-made)
Recombinant protein: Shank3-NTD-ANK-K22A+R72E (aa 1-376)	This paper	N/A (custom-made)
Recombinant protein: Shank3-NTD (aa 1-104)	This paper	N/A (custom-made)
Recombinant protein: Shank3-NTD-R12E (aa 1-104)	This paper	N/A (custom-made)
Recombinant protein: Shank3-NTD-K22E (aa 1-104)	This paper	N/A (custom-made)
Recombinant protein: Shank3-NTD-K22A (aa 1-104)	This paper	N/A (custom-made)
Recombinant protein: Shank3-NtoSAM (aa 1-376 + 533-665 + 1294-1323 + 1400-1426 + 1654-1730)	This paper	N/A (custom-made)
Recombinant protein: SynGAP-C2-GAP (aa 244-740)	This paper	N/A (custom-made)
Recombinant protein: p120GAP-GAP (aa 714-1047)	This paper	N/A (custom-made)
Recombinant protein: HRas (aa 1-167)	This paper	N/A (custom-made)
Recombinant protein: Rap1b (aa 1-167)	This paper	N/A (custom-made)
Recombinant protein: Rap2a (aa 1-167)	This paper	N/A (custom-made)
Recombinant protein: RRas (aa 22-201)	This paper	N/A (custom-made)
Recombinant protein: MRas (aa 10-178)	This paper	N/A (custom-made)
Recombinant protein: Trx-SAPAP-CT	(Zeng et al., 2016)	N/A (custom-made)
Recombinant protein: Homer1a	(Zeng et al., 2018)	N/A (custom-made)
Deposited Data		
Crystal structure of Shank3 NTD-ANK/Rap1 complex	This paper	PDB: 6KYK
Crystal structure of Shank3 NTD-ANK/HRas complex	This paper	PDB: 6KYH
Experimental Models: Organisms/Strains		
Rat: SD.	SLC	N/A
Escherichia coli: BL21-CodonPlus(DE3)-RIL	Agilent	Cat#230245
Recombinant DNA		
Plasmid: 32mTEV-Shank1-NTD-ANK (aa 73-440)	This paper	N/A
Plasmid: 32m3c-Shank2-NTD-ANK (aa 49-423)	This paper	N/A
Plasmid: 32m3c-Shank3-NTD-ANK (aa 1-376)	This paper	N/A
Plasmid: 32m3c-Shank3-NTD-ANK (aa 1-368)	This paper	N/A
Plasmid: 32m3c-Shank3-NTD-ANK (aa 1-362)	This paper	N/A
Plasmid: 32m3c-Shank3-NTD-ANK-A42K (aa 1-362)	This paper	N/A

(Continued on next page)

Continued

REAGENT or RESOURCE	SOURCE	IDENTIFIER
Plasmid: 32m3c-Shank3-NTD-ANK-C41K+A42K (aa 1-362)	This paper	N/A
Plasmid: 32m3c-Shank3-NTD-ANK- Δ CT (aa 1-348)	This paper	N/A
Plasmid: 32m3c-Shank3-NTD-ANK-K22A (aa 1-376)	This paper	N/A
Plasmid: 32m3c-Shank3-NTD-ANK-K66E (aa 1-376)	This paper	N/A
Plasmid: 32m3c-Shank3-NTD-ANK-R72E (aa 1-376)	This paper	N/A
Plasmid: 32m3c-Shank3-NTD-ANK-K22A+R72E (aa 1-376)	This paper	N/A
Plasmid: 32m3c-Shank3-NTD (aa 1-104)	This paper	N/A
Plasmid: 32m3c-Shank3-NTD-R12E (aa 1-104)	This paper	N/A
Plasmid: 32m3c-Shank3-NTD-K22E (aa 1-104)	This paper	N/A
Plasmid: 32m3c-Shank3-NTD-K22A (aa 1-104)	This paper	N/A
Plasmid: MG3c-Shank3-NtoSAM (aa 1-376 + 533-665 + 1294-1323 + 1400-1426 + 1654-1730)	This paper	N/A
Plasmid: MG3c-SynGAP-C2-GAP (aa 244-740)	This paper	N/A
Plasmid: m3c-p120GAP-GAP (aa 714-1047)	This paper	N/A
Plasmid: m3c-HRas (aa 1-167)	This paper	N/A
Plasmid: pskB2-Rap1b (aa 1-167)	This paper	N/A
Plasmid: pskB2-Rap2a (aa 1-167)	This paper	N/A
Plasmid: pskB2-RRas (aa 22-201)	This paper	N/A
Plasmid: pskB2-MRas (aa 10-178)	This paper	N/A
Plasmid: 32m3c-SAPAP-CT	(Zeng et al., 2016)	N/A
Plasmid: m3c-Homer1a	(Zeng et al., 2018)	N/A
Plasmid: pEGFP-Shank3 full length	This paper	N/A
Plasmid: pmCherry-Rap1 full length	This paper	N/A
Plasmid: pmCherry-HRas full length	This paper	N/A
Software and Algorithms		
Origin 7.0	OriginLab	http://www.originlab.com/
HKL2000 & HKL3000	(Otwinowski and Minor, 1997)	http://www.hkl-xray.com/
ASTRA 6	Wyatt	http://www.wyatt.com/products/software/astra.html
Coot	(Emsley et al., 2010)	http://www2.mrc-lmb.cam.ac.uk/Personal/pemsley/coot/
Refmac5	(Murshudov et al., 2011)	https://www2.mrc-lmb.cam.ac.uk/groups/murshudov/
MolProbity	(Chen et al., 2010)	http://molprobity.biochem.duke.edu/
PyMOL	Schrödinger, LLC	https://www.pymol.org/
Prism	GraphPad	https://www.graphpad.com/scientific-software/prism/
ImageJ	NIH	https://imagej.nih.gov/ij/
SPCImage	Becker & Hickl	https://www.becker-hickl.com/
Igor Pro	Wave Metrics	https://www.wavemetrics.com
Excel	Microsoft	https://products.office.com/
Real Statistics Resource Pack	Charles Zaiontz	http://www.real-statistics.com/

LEAD CONTACT AND MATERIALS AVAILABILITY

Further information and requests for resources and reagents should be directed to and will be fulfilled by the Lead Contact, Mingjie Zhang (mzhang@ust.hk). This study did not generate new unique reagents.

EXPERIMENTAL MODEL AND SUBJECT DETAILS

All experimental protocols were approved by the Kyoto University Committee for Animal Care guidelines.

Animals

Rats from Sprague-Dawley strain (purchased Japan SLC, both males and females) were used for hippocampal slice culture and dissociated neuronal cultures.

Bacterial Strain

Escherichia coli BL21-CodonPlus(DE3)-RIL cells (Agilent) were used in this study for the production of recombinant proteins. Cells were cultured in LB medium supplemented with necessary antibiotics.

METHODS DETAILS

Constructs

The cDNA encoding mouse Shank1 (Genbank: NM_031751.3) NTD-ANK fragment (residues 73-440), HRas (Genbank: AY373386.1, residues 1-167) and SynGAP (Uniprot: J3QQ18) were PCR-amplified from a mouse cDNA library. The human Shank2 NTD-ANK fragment (residues: 49-423) was PCR-amplified from the full-length Shank2 gene (Genbank: NM_012309) purchased from YouBio Co. Various fragments of mouse Shank3 were PCR-amplified from the full-length Shank3 gene (Genbank: AB231013), provided Prof. Guoping Feng at Massachusetts Institute of Technology. NtoSAM was generated by using overlap PCR method to fuse multiple Shank3 cDNA fragments, including residues 1-376, 533-665, 1294-1323, 1400-1426 and 1654-1730. The SynGAP C2-GAP fragment (residues 244-740) was PCR-amplified from the full-length rat SynGAP (Uniprot: Q9QUH6), provided by Prof. Richard Huganir at Johns Hopkins University School of Medicine. Human RRas (residues 22-201), Rap1b (residues 1-167), Rap2a (residues 1-167), p120GAP (residues 714-1047) and mouse MRas (residues 10-178) genes were provided by Prof. Xuewu Zhang in UT Southwestern Medical Center.

Each of the Shank fragments was inserted into a modified pET-32a vectors with a N-terminal Trx-His₆ and a TEV protease cutting site (for Shank1) or an HRV-3C protease cutting site (for Shank2 and Shank3). For Shank3 NTD-ANK and its derivatives, two point mutations, L231R and F304Y, were incorporated to improve the quality of recombinant proteins. These two mutations are far away from the small GTPases binding sites and do not have any impact on the binding to Rap1 and HRas to Shank3. All small GTPases were cloned into a vector with N-terminal hexahistidine tag followed by an HRV-3C protease cutting site. SynGAP C2-GAP fragment and Shank3 NtoSAM were cloned into a vector with an N-terminal GB1-His₆ and an HRV-3C protease cutting site. For the FRET-FLIM experiments, full-length Shank3 gene was cloned into pEGFP-C3 vector with N-terminal EGFP tag. Full-length Rap1b and HRas genes were each cloned into pEGFP-C3 vector and N-terminal EGFP tag was replaced by mCherry. Mutants were generated by a standard PCR-based method. All constructs were confirmed by DNA sequencing.

Protein Expression and Purification

All proteins were expressed in *Escherichia coli* BL21-CodonPlus(DE3)-RIL cells (Agilent Technologies) in LB medium at 16°C. Recombinant proteins were firstly purified using Ni²⁺-NTA resin (GE Healthcare). Then Superdex 200 26/60 or Superdex 75 26/60 gel filtration columns were used for further purifications. The affinity tag of each protein was cleaved by HRV-3C protease or TEV protease at 4°C overnight and removed by another step of gel filtration chromatography in the buffer containing 50 mM Tris (pH 8.0), 50 mM NaCl, 50 mM ammonium tartrate, 2 mM DTT and 2 mM MgCl₂.

The active (GMPPNP-bound) form of small GTPases was generated according to the previous reported protocol (John et al., 1990). Briefly, each purified small GTPase was exchanged into the buffer containing 50 mM Tris, pH 8.0, 100 mM NaCl, 200 mM ammonium sulfate, 2 mM DTT, then concentrated to 100 μM. GMPPNP and alkaline phosphatase (NEB) were added to reach final concentrations of 500 μM and 2 units/mg GTPase, respectively. After incubated at 4°C overnight, the protein was desalted into the buffer containing 50 mM Tris (pH 8.0), 50 mM NaCl, 50 mM ammonium tartrate, 2 mM DTT and 2 mM MgCl₂. The GDP-bound small GTPase was prepared by incubating purified small GTPases with corresponding GAP protein (SynGAP C2-GAP for Rap1 and p120GAP for the rest of small GTPases) for 24 h at 4°C in the buffer containing 50 mM Tris, pH 8.0, 100 mM NaCl, 2 mM DTT and 2 mM MgCl₂. Then small GTPases were further purified by a step of gel filtration chromatography.

Protein Crystallization and Structure Determination

All crystals were obtained by hanging drop vapor-diffusion method at 16°C. Shank3 NTD-ANK (residues 1-368) and Rap1b (residues 1-167) were mixed at a molar ratio of 1:2 with the concentration of 15 mg/mL for crystallization. Crystals of Shank3 and Rap1 complex were grown in the condition containing 0.1 M bicine (pH8.5), 1% Dextran sulfate sodium salt, 5% PEG 20000, 10% PEG 1500. Shank3 NTD-ANK (residues 1-362) A42K mutant and HRas (residues 1-167) were mixed at a molar ratio of 1:1.5 with the concentration of 12 mg/mL for crystallization. Crystals of Shank3 and HRas complex were grown in the condition containing 0.1 M bicine (pH8.5), 3% Dextran sulfate sodium salt, 15% PEG 20000.

Crystals were cryoprotected with 30 % (v/v) glycerol and flash-cooled to 100 K. X-ray diffraction data were collected at BL17U1 or BL19U1 beamlines at Shanghai Synchrotron Radiation Facility (SSRF). Diffraction data were processed using HKL2000 or HKL3000 (Otwinowski and Minor, 1997). Structures were solved by molecular replacement method using Phaser (McCoy et al., 2007). The crystal structures of Shank3 NTD-ANK (PDB ID: 5G4X), Rap1b (PDB ID: 4DXA) and HRas (PDB ID: 6AMB) were used as the searching models. For Shank3 NTD-ANK/Rap1 complex structure, two Shank3 NTD-ANK molecules and four Rap1b molecules could be found in an asymmetric unit. For Shank3 NTD-ANK-A42K/HRas complex structure, four Shank3 NTD-ANK molecules and four HRas

molecules could be found in an asymmetric unit. Manual model building and refinement were carried out iteratively using Coot (Emsley et al., 2010) and Refmac5 (Murshudov et al., 2011). High resolution crystal structures of Shank3 NTD-ANK, Rap1b and HRas were used as references to generate external restraints during refinement. The final models were validated by MolProbity (Chen et al., 2010) and statistics were summarized in Table 1. The figures were produced using PyMOL (<http://www.pymol.org/>).

Isothermal Titration Calorimetry (ITC) Assay

ITC experiments were carried out using a VP-ITC calorimeter (Malvern) at 25°C. All proteins used in ITC experiments were in the buffer containing 50 mM Tris (pH 8.0), 50 mM NaCl, 50 mM ammonium tartrate, 2 mM DTT and 2 mM MgCl₂. Each titration point was performed by injecting a 10 μ l aliquot of one protein in the syringe into its binding protein in the cell at a time interval of 120 s to ensure that the titration peak returned to the baseline. Titration data were fitted with the one-site binding model using Origin 7.0 to get the apparent K_d values.

GAP Activity Assay

The EnzChek phosphate assay kit (E6646, ThermoFisher) was employed to monitor the GAP activity. 20 μ M small GTPases (including HRas, RRas, MRas, Rap1, Rap2) with 5 μ M SynGAP C2-GAP were added into the reaction solution containing 50 mM Tris (pH8.0), 100 mM NaCl, 2 mM DTT, 5mM EDTA, 150 μ M GTP, 1 U/ml purine nucleoside phosphorylase (PNP) and 200 μ M 2-amino-6-mercapto-7-methylpurine riboside (MESG) to study the specificity of SynGAP. Then 20 μ M Rap1 with or without 5 μ M SynGAP-C2-GAP was added into the same condition with 10 μ M or 20 μ M Shank3 NTD-ANK mutants to study the influence of Shank3 on the GAP activity of SynGAP. The absorbance at 360 nm was measured every 5 s in a 1 cm path-length cuvette at 25°C for 40 min using a UV spectrophotometer (UV-1800, Shimadzu). The data were fitted with one phase association equation with shared plateau using GraphPad Prism to derive the K_{obs} values.

Glutamate Uncaging and Fluorescent Lifetime Imaging

Glutamate uncaging and FRET-FLIM observation using hippocampal slice was described previously (Bosch et al., 2014; Saneyoshi et al., 2019). Briefly, 5-6 DIV hippocampal organotypic slice cultures were transfected by biolistic method (Gene-Gun, Bio-Rad, CA, USA) with GFP-Shank3, mCherry-Rap1 or mCherry-HRas and DsRed plasmids at a 2:3:1 ratio. At 10-12 DIV, imaging was carried out in Mg²⁺-free artificial cerebrospinal fluid (ACFS) containing 4 mM CaCl₂, 1 μ M tetrodotoxin, 50 μ M picrotoxin, and 2.5 mM MNI-caged-L-glutamate aerated with 95% O₂ and 5% CO₂ using two-photon microscope (FV1000-MPE, Olympus, Tokyo, Japan) and Ti-sapphire lasers (Spectra-Physics, CA, USA). Glutamate uncaging was performed on the dendritic spines at primary or secondary dendrites from the distal part of the main apical dendrite of CA1 pyramidal neurons with 2 ms 2-photon laser pulses (720 nm at 5 mW under objective lens) repeated at 0.5 Hz for 60 sec. Fluorescent lifetime of GFP-Shank3 was measured by time-correlated photon-counting technology (SPC-830, Becker and Hickl, Berlin, Germany; H7422P-40, Hamamatsu Photonics, Hamamatsu, Japan) at 910 nm excitation. Emission light was filtered with a 680 nm short-pass and 510/70 nm band-pass filters. The lifetime images were analyzed using SPC image (Becker and Hickl, Berlin, Germany) and a custom written macro in Igor-Pro (Wavemetrics, OR, USA). Averaged fluorescence lifetime in the spine head was calculated and presented as the difference from baseline.

QUANTIFICATION AND STATISTICAL ANALYSIS

Statistical parameters including the definitions and exact values of n are reported in the figures and corresponding figure legends. The statistical significance of the results was assessed using one-way ANOVA with Scheffé's post hoc comparison. P < 0.05 was considered significant. Statistical analysis was performed in Real Statistics Resource Pack for Excel (Microsoft).

DATA AND CODE AVAILABILITY

The atomic coordinates of Shank3 NTD-ANK/Rap1 complex and Shank3 NTD-ANK/HRas complex have been deposited to the Protein Data Bank (PDB) with the accession numbers of 6KYK and 6KYH, respectively.